Anal. Chem. **2008,** *80,* 3270−3276

Enzymatic Reactions in Microfluidic Devices: Michaelis−Menten Kinetics

William D. Ristenpart, Jiandi Wan, and Howard A. Stone*

School of Engineering and Applied Sciences, Harvard University, Cambridge, Massachusetts 02138

Kinetic rate constants for enzymatic reactions are typically measured with a series of experiments at different substrate concentrations in a well-mixed container. Here we demonstrate a microfluidic technique for measuring Michaelis−Menten rate constants with only a single experiment. Enzyme and substrate are brought together in a coflow microfluidic device, and we establish analytically and numerically that the initial concentration of product scales with the distance x along the channel as $x^{5/2}$. Measurements of the initial rate of product formation, combined with the quasi-steady rate of product formation further downstream, yield the rate constants. We corroborate the $x^{5/2}$ scaling result experimentally using the bioluminescent reaction between ATP and luciferase/luciferin as a model system.

Enzymatic reactions, wherein one reacting species serves as a catalyst for converting another species into a desired product, are ubiquitous in biological systems. Accordingly, accurate measurements of the rate constants associated with specific enzymatic reactions are crucial for applications in biochemistry, medicine, food science, and biochemical engineering. Many enzymatic reactions are characterized by the Michaelis−Menten[1] reaction scheme

$$\mathrm{E} + \mathrm{S} \underset{k_2}{\overset{k_1}{\rightleftharpoons}} \mathrm{E{\cdot}S} \xrightarrow{k_{\mathrm{cat}}} \mathrm{E} + \mathrm{P} \qquad (1)$$

where E, S, and P represent, respectively, the enzyme, substrate, and product. In a well-mixed system, the initial rate of product formation (i.e., the reaction "velocity") is

$$\left.\frac{\mathrm{d[P]}}{\mathrm{d}t}\right|_{\mathrm{i}} = k_{\mathrm{cat}}[\mathrm{E}]_{\mathrm{i}}\left(\frac{[\mathrm{S}]_{\mathrm{i}}}{K_{\mathrm{m}} + [\mathrm{S}]_{\mathrm{i}}}\right) \qquad (2)$$

provided that the concentration of intermediate species E·S is quasi-steady.[2] Here the subscript "i" denotes the initial concentration or reaction rate, and $K_{\mathrm{m}} \equiv (k_{\mathrm{cat}} + k_2)/k_1$ is the so-called Michaelis constant, with dimensions of concentration. The constant K_{m} serves as an important indicator of whether the reaction rate is limited by the amount of substrate (i.e., $[\mathrm{S}]_{\mathrm{i}} \ll K_{\mathrm{m}}$) or by the enzyme being saturated ($[\mathrm{S}]_{\mathrm{i}} \gg K_{\mathrm{m}}$). Consequently, determination of K_{m} is a primary objective of kinetic analyses on enzymatic reactions. The conventional method to determine K_{m} is to measure the initial reaction rate for many different initial substrate concentrations $[\mathrm{S}]_{\mathrm{i}}$ and to fit the data to eq 2. This approach requires multiple separate experiments to yield accurate measurements of K_{m}.

In this work we propose a different approach, based on a coflow microfluidic device, which yields the enzymatic rate constants k_1 and k_{cat} with a single experiment. The advantages and general features of microfluidic devices have been widely discussed;[3,4] a key advantage is the possibility of measuring rate constants with substantially reduced amounts of enzyme compared to standard techniques. Previous work on coflow microfluidic devices[5−11] has focused on reactions of the form $\mathrm{A} + \mathrm{B} \overset{K_{\mathrm{eq}}}{\longleftrightarrow} \mathrm{C}$, where A and B are brought together at a Y-shaped junction (cf. Figure 1). Provided the channel dimensions are sufficiently small, then the flow is laminar and the species slowly diffuse toward one another (transverse to the primary flow direction) and then react to form C. The kinetic parameters are determined by measuring [C] as a function of position downstream from the junction. For small molecules with comparable diffusivities, however, there is no straightforward procedure to extract rate constants from the experimental data; the rate constants must be treated as fitting parameters in numerical computations of the full set of reaction−diffusion equations. Reliance on numerical calculations is inconvenient for experimentalists, so a compact analytical solution is desirable.

Here we demonstrate that under appropriate conditions the governing equations, accounting for convection, diffusion, and reaction, are simplified and a simple power-law solution is obtained for the spatial evolution of the product concentration. Specifically, analytical and numerical calculations show that the product

* Corresponding author. Phone: (617) 495-3599. E-mail: has@seas.harvard.edu.

(1) Michaelis, L.; Menten, M. L. *Biochem. Z.* **1913**, *49*, 333.
(2) Bailey, J. E.; Ollis, D. F. *Biochemical Engineering Fundamentals*; McGraw-Hill Inc.: New York, 1986.
(3) Stone, H. A.; Stroock, A. D.; Ajdari, A. *Annu. Rev. Fluid Mech.* **2004**, *36*, 381.
(4) Squires, T. M.; Quake, S. R. *Rev. Mod. Phys.* **2005**, *77*, 977.
(5) Kamholz, A. E.; Weigl, B. H.; Finlayson, B. A.; Yager, P. *Anal. Chem.* **1999**, *71*, 5340.
(6) Kamholz, A. E.; Schilling, E. A.; Yager, P. *Biophys. J.* **2001**, *80*, 1967.
(7) Kamholz, A. E.; Yager, P. *Biophys. J.* **2001**, *80*, 155.
(8) Baroud, C. N.; Okkels, F.; Menetrier, L.; Tabeling, P. *Phys. Rev. E* **2003**, *67*, 060104R.
(9) Salmon, J. B.; Dubrocq, C.; Tabeling, P.; Charier, S.; Alcor, D.; Jullien, L.; Ferrage, F. *Anal. Chem.* **2005**, *77*, 3417.
(10) Benninger, R. K. P.; Hofmann, O.; Önfelt, B.; Munro, I.; Dunsby, C.; Davis, D. M.; Neil, M. A. A.; French, P. M. W.; de Mello, A. J. *Angew. Chem., Int. Ed.* **2007**, *46*, 2228.
(11) Matthews, S. M.; Elder, A. D.; Yunus, K.; Kaminski, C. F.; Brennan, C. M.; Fisher, A. C. *Anal. Chem.* **2007**, *79*, 4101.

10.1021/ac702469u CCC: $40.75
Published on Web 03/21/2008

concentration scales in the downstream x direction as $x^{5/2}$, with a prefactor proportional to $k_1 k_{cat}$. Further downstream the species are well mixed, and for sufficiently high initial substrate concentrations the product concentration scales linearly in x with a slope proportional to k_{cat}. Thus, measuring the product concentration as a function of position both near and far from the Y-junction yields the desired rate constants, without necessitating comparison to numerical calculations. Moreover, the necessary measurements can be accomplished in a single microfluidic experiment.

We first summarize the governing equations and provide a scaling argument for the $x^{5/2}$ power law. Numerical and experimental results then follow, and we close with a discussion of possible extensions to more complicated reactions.

Reaction-Diffusion Model and Power-Law Scaling. We consider a pressure-driven flow along the x-axis of a microfluidic system with width w and depth h (cf. Figure 1). The laminar flow profile inside a microfluidic channel depends in general on both y and z. In microchannels with large aspect ratio ($w/h \gg 1$), however, the flow is mainly uniform in the y-direction and parabolic in the z-direction. Because of the parabolic profile, in general the species concentrations are not uniform in the z-direction;[12,13] the concentration profiles near the top and bottom of the channel (where the velocity is lowest) are different compared to the center of the channel. As a first approximation, we neglect this complexity and focus on the behavior near the center of the channel ($z \approx h/2$) where the species concentrations are relatively uniform. In this case, the reaction−diffusion process may be modeled as two-dimensional.

Moreover, we assume that convective transport by a mean fluid velocity u dominates over diffusive transport in the downstream x-direction. This assumption is valid if the Peclet number $\mathrm{Pe} = uh/D$ is large, as is representative of most microfluidic conditions (e.g., for a system with $u \approx 10^{-2}$ m/s, $h \approx 10^{-4}$ m and $D = 10^{-9}$ m^2/s, the Peclet number is 10^3). In this situation, the governing equations for the steady-state concentrations of each species involved in the enzymatic reaction are

$$\text{substrate:}\quad u\frac{\partial[\mathrm{S}]}{\partial x} = D_\mathrm{S}\frac{\partial^2[\mathrm{S}]}{\partial y^2} - k_1[\mathrm{S}][\mathrm{E}] + k_2[\mathrm{E{\cdot}S}] \quad (3)$$

$$\text{enzyme:}\quad u\frac{\partial[\mathrm{E}]}{\partial x} = D_\mathrm{E}\frac{\partial^2[\mathrm{E}]}{\partial y^2} - k_1[\mathrm{S}][\mathrm{E}] + (k_2 + k_{cat})[\mathrm{E{\cdot}S}] \quad (4)$$

$$\text{intermediate:}\quad u\frac{\partial[\mathrm{E{\cdot}S}]}{\partial x} = D_{\mathrm{E{\cdot}S}}\frac{\partial^2[\mathrm{E{\cdot}S}]}{\partial y^2} + k_1[\mathrm{S}][\mathrm{E}] - (k_2 + k_{cat})[\mathrm{E{\cdot}S}] \quad (5)$$

$$\text{product:}\quad u\frac{\partial[\mathrm{P}]}{\partial x} = D_\mathrm{P}\frac{\partial^2[\mathrm{P}]}{\partial y^2} + k_{cat}[\mathrm{E{\cdot}S}] \quad (6)$$

Here D_j is the diffusivity of species j. This description is essentially the basis of the Michaelis−Menten model, where the time derivatives are replaced with spatial derivatives and with the additional complexity of the transverse diffusive terms. At the entrance of the Y-shaped junction, looking in the x-direction the substrate is introduced on the right-hand side ($y < 0$) and the enzyme on the left ($y > 0$), while the intermediate and product concentrations on both sides are assumed to be zero. Thus, the initial conditions are those for initially separated species,

$$x = 0:\quad [\mathrm{S}] = \begin{cases} 0 & y > 0 \\ [\mathrm{S}]_\mathrm{i} & y < 0 \end{cases} \qquad [\mathrm{E}] = \begin{cases} [\mathrm{E}]_\mathrm{i} & y > 0 \\ 0 & y < 0 \end{cases}$$
$$[\mathrm{E{\cdot}S}] = 0 \qquad [\mathrm{P}] = 0 \quad (7)$$

where the subscript i denotes the initial concentration.

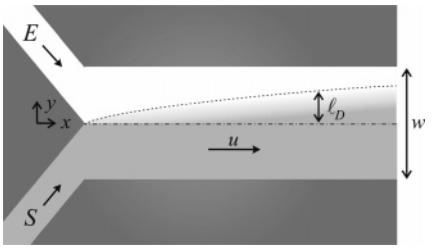

Figure 1. Schematic of a microfluidic Y-junction used for experiments to measure enzymatic rate constants. The channel depth h is in the z-direction oriented out of the page.

The system of eqs 3−7 is readily solved numerically by standard methods but with appropriate simplifications, consistent with typical experimental conditions, a compact analytical result is obtained. The two key assumptions are (i) a small enzyme diffusivity and (ii) a small reaction rate. Most enzymes are significantly larger than their respective substrates; for example, the molecular weight of firefly luciferase is 61 kDa while ATP is only 0.5 kDa, yielding $D_\mathrm{E}/D_\mathrm{S} \approx 0.2$. Since the intermediate species is necessarily larger than the enzyme itself, it follows that the diffusivity of the intermediate species is likewise small. Thus, when the enzyme and substrate are brought together at a Y-junction, the substrate rapidly diffuses in the y direction toward the enzyme, while the enzyme remains relatively confined to its original side of the channel. Accordingly, we neglect the transverse diffusion of the enzyme and intermediate species close to the junction, and the concentration of intermediate species is approximately governed by a balance between convection and the forward reaction, i.e., the first and third terms in eq 4. Note that the back reaction is negligible for small values of x because the initial concentration of E·S is small. This approximation requires that the concentration of intermediate species varies with position as

$$[\mathrm{E{\cdot}S}] \approx \frac{k_1[\mathrm{S}][\mathrm{E}]x}{u} \quad (8)$$

To make further progress, estimates of [S] and [E] as functions of x are required.

As a second key simplification, we focus on systems where the rate of depletion of substrate and enzyme by chemical reaction rate is "small" compared to the influence of diffusion and convection. A precise definition of small is obtained via a formal perturbation analysis,[14] which indicates that the reaction terms in eqs 3 and 4 are negligible if the inequality $k_1[\mathrm{E}]_\mathrm{i}D_\mathrm{S}/u^2 \ll 1$ is

(12) Ismagilov, R. F.; Stroock, A. D.; Kenis, P. J. A.; Whitesides, G.; Stone, H. A. *Appl. Phys. Lett.* **2000**, *76*, 2376.
(13) Salmon, J. B.; Ajdari, A. *J. Appl. Phys.* **2007**, *101*, 074902.
(14) Ristenpart, W. D.; Wan, J.; Stone, H. A. Manuscript in preparation.

satisfied. Given the representative values $D_S \approx 10^{-9}$ m^2/s and $u \approx 10^{-2}$ m/s, and a practical upper bound of $[E]_i < 10^{-3}$ M, this inequality is satisfied if $k_1 \ll 10^8$ M^{-1} s^{-1}, which covers a wide variety of enzymatic reactions.[2] Note that the forward reaction term is not negligible in eq 5 because the intermediate species is only present due to the chemical reaction. With diffusion and the reaction both negligible, the governing equation for the enzyme (eq 4) simplifies to $\partial[E]/\partial x \approx 0$ and the concentration of enzyme is simply $[E] = [E]_i$. Thus, the enzyme is confined to its original side of the channel at its original concentration.

In contrast, for a negligible reaction rate but non-negligible diffusion, eq 3 simplifies to

$$u\frac{\partial[S]}{\partial x} \approx D_S\frac{\partial^2[S]}{\partial y^2} \tag{9}$$

This equation has a well-known analytical solution, which serves as the basis of a formal perturbation analysis.[14] Here we simply note that the extent of diffusion in the y-direction is described by the classic convective−diffusive length scale $l_D = \sqrt{D_S x/u}$. In other words, for sufficiently small x the length scale l_D provides an estimate of how far the substrate has diffused into the enzyme-rich side of the channel (cf. Figure 1).

To estimate the reaction rate, however, we require an estimate of *how much* substrate has diffused into the enzyme-rich side, rather than *how far*. In the absence of significant depletion by chemical reaction, conservation of mass requires that the integral amount of substrate be conserved. We therefore define an integral average concentration ⟨S⟩, given by integrating the volumetric concentration over both the width and height of the channel. Note ⟨S⟩ has dimensions of moles per length of channel and is a function of x; comparable definitions apply for the other species. In terms of a scaling estimate for the enzyme side of the channel ($y > 0$), we obtain

$$\langle S\rangle \approx h[S]_i l_D = h[S]_i\sqrt{\frac{D_S x}{u}} \tag{10}$$

since l_D represents the width of the region with nonzero substrate concentration. This estimate is only valid for small x where the applicable values of y (i.e., where the concentration is nonzero) are small compared to the width of the channel. Substitution of this estimate for ⟨S⟩ into eq 8 yields the scaling expression

$$\langle E{\cdot}S\rangle \approx \frac{k_1 h[E]_i[S]_i l_D}{u}x = \frac{k_1 h[E]_i[S]_i {D_S}^{1/2}}{u^{3/2}}x^{3/2} \tag{11}$$

Now that we have the intermediate concentration, we may substitute it into eq 6. After integration with respect to x, we obtain

$$\langle P\rangle \approx \frac{k_1 k_{cat} h[E]_i[S]_i {D_S}^{1/2}}{u^{5/2}}x^{5/2} \tag{12}$$

The same result (with a different numerical prefactor) is obtained via a formal perturbation analysis.[14] We stress that eq 12 represents the average amount of product, with dimensions of moles per length, at a specific x-position along the channel. Note that according to eq 12, the concentration of product increases linearly with the initial concentrations of substrate and enzyme, consistent with the reaction scheme in eq 1. Likewise, the product concentration scales linearly with the rate constants k_1 and k_{cat}. The reverse binding rate constant k_2 does not affect the product concentration, however, because the influence of the reverse reaction is negligible at early times. Not surprisingly, the amount of product depends on the substrate diffusivity, which controls how quickly the substrate diffuses into the enzyme, and is quite sensitive to the average fluid velocity. Increasing the velocity decreases the amount of product at a given value of x because the reactants are pushed further downstream before they are able to react.

The preceding analysis focused on the formation of product close to the junction where enzyme and substrate are first brought together. In this region, the species are not well mixed and the diffusivity of the substrate limits the reaction. Sufficiently far downstream, however, all of the species are completely mixed by diffusion. In this region, all of the diffusive terms in eqs 3−6 vanish, so the governing equations reduce to those used in the classic Michaelis−Menten analysis, with the time derivatives recast as spatial derivatives in the moving reference frame. Hence, we employ the usual assumption that the concentration of intermediate species is quasi-steady, i.e., $\partial[E{\cdot}S]/\partial x = 0$, and note that $[E{\cdot}S] = [E]_i - [E]$ to obtain

$$u\frac{d[P]}{dx} = k_{cat}[E]_i\left(\frac{[S]}{K_m + [S]}\right) \tag{13}$$

This equation has the same form as the Michaelis−Menten result (cf. eq 2). Here, however, we are interested in the reaction rate far downstream, so unlike in the classic result the relevant substrate concentrations in eq 13 are *not* the initial values. Generally speaking, the reaction rate will decrease as the reaction progresses since [S] necessarily decreases. Because [S] is unknown, eq 13 is not helpful for predicting the reaction rate for arbitrary substrate concentrations. Nonetheless, if the substrate concentration far downstream is still large compared to K_m, then from eq 13 the reaction rate no longer depends on the specific value of [S], and the product concentration scales linearly with x, viz.,

$$[P] \approx \frac{k_{cat}[E]_i}{u}x, \quad \text{large } x \text{ and } \quad [S] \gg K_m \tag{14}$$

This result is analogous to the "maximum velocity" found in the classic Michaelis−Menten analysis for very high substrate concentrations. If the initial enzyme concentration and velocity in the microfluidic channel are known, then k_{cat} is readily determined. Once k_{cat} is known, k_1 is then obtained by fitting the upstream concentrations to $x^{5/2}$ using eq 12.

We emphasize that the procedure described above, i.e., fitting the measured product concentration both near and far from the junction to eqs 12 and 14, respectively, will only be valid for reactions that are described by standard Michaelis−Menten kinetics. The product must not be depleted by subsequent reactions (as is the case with luciferase, see below) nor by any

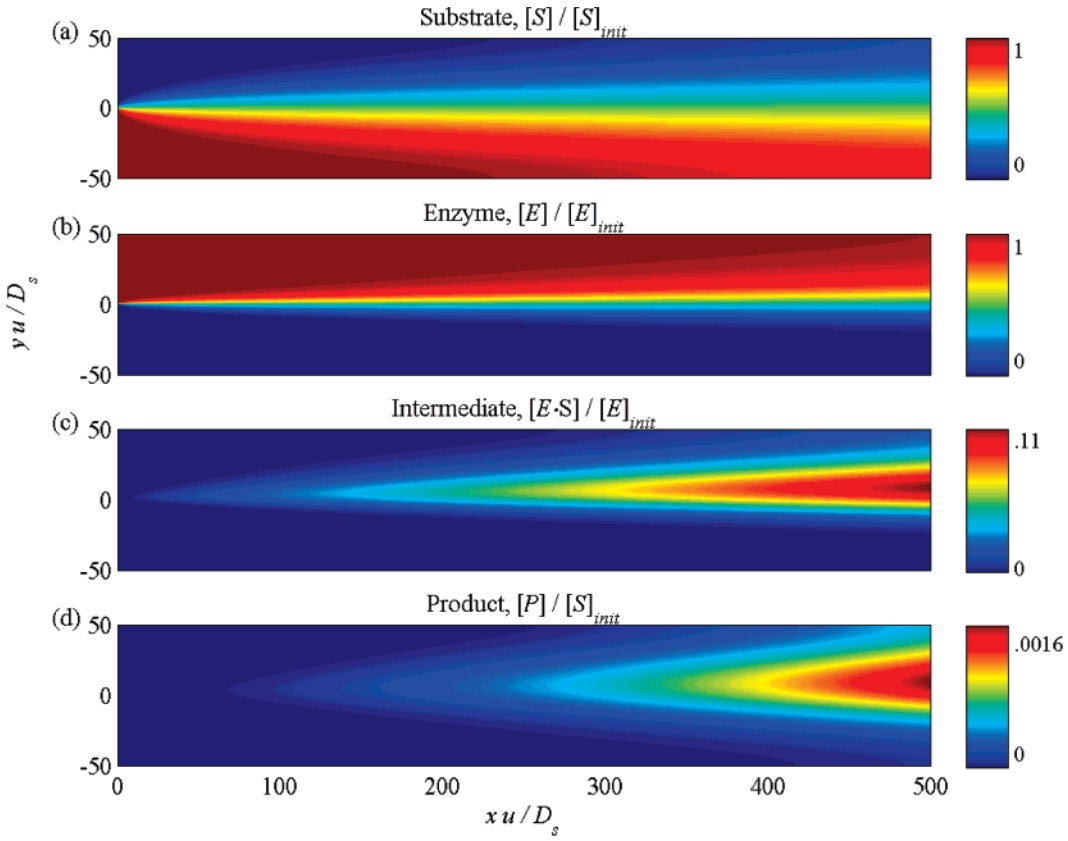

Figure 2. Numerically calculated contour plots of the scaled concentration of each species in the enzymatic reaction near the entrance of a Y-junction microfluidic channel. Substrate enters from the lower part of the channel ($y < 0$), while enzyme enters near the upper part ($y > 0$). Dark blue is zero concentration, red is high concentration. Flow is in the positive x-direction (left to right). The substrate diffuses rapidly compared to the enzyme, so the intermediate and product species are produced almost entirely on the enzyme side of the channel. Parameters for numerical calculations are specified in Table 1.

Table 1. Typical Parameters for Numerical Calculations

D_E, $D_{E\cdot S}$	10^{-10} m^2 s^{-1}	u	10^{-2} m s^{-1}
D_S, D_P	10^{-9} m^2 s^{-1}	k_1	10^4 M^{-1} s^{-1}
$[S]_i$	10^{-2} M	k_2	10^0 s^{-1}
$[E]_i$	10^{-6} M	k_{cat}	10^1 s^{-1}

reverse reaction of product back to an intermediate state. Furthermore, the amount of substrate consumed in the upstream part of the channel should be small; as shown rigorously elsewhere,[14] this condition is satisfied if $[S]_i \gg k_{cat}[E]_i w^2/D_E$, which is readily achieved experimentally.

Numerical Calculations. Equations 3−7 were solved numerically in Matlab using standard methods. No-flux boundary conditions were applied at fixed values of $y = \pm w$, where $W = wu/D_S = 50$ was chosen as a representative width; changes in W did not affect the results qualitatively. Representative values of the initial concentrations, rate constants, and diffusivities were chosen based on reported values for the reaction between ATP and firefly luciferase[15] and are listed in Table 1. For each series of numerical calculations, all parameters were fixed at the values specified in Table 1 except for the systematically varied parameter.

Representative contour plots of the concentration of each species versus $X = xu/D_S$ and $Y = yu/D_S$ are presented in Figure 2. From this perspective, the substrate is entering from the bottom (i.e., $y < 0$) while the enzyme enters along the top ($y > 0$). Because of its higher diffusivity, the substrate rapidly spreads in the transverse direction (Figure 2a), while the slower enzyme stays relatively confined to its original side of the channel (Figure 2b). Because the rate of binding between substrate and enzyme is sufficiently slow and the initial substrate concentration is sufficiently large, comparatively little of the substrate and enzyme are consumed by reactions. Thus, to a good approximation both the substrate and enzyme concentrations are (at these early stages) governed entirely by diffusion.

In contrast, the intermediate species E·S can only form where the concentrations of enzyme and substrate are both nonzero. Thus, E·S appears only on the enzyme side of the channel in regions where the substrate concentration has increased appreciably by diffusion (Figure 2c). The profile of the resulting E·S contours is consequently asymmetric, growing in the positive y-direction as the substrate penetrates further into the enzyme side of the channel. The concentration of product is similarly asymmetric, since it is only produced wherever E·S is formed (Figure 2d). Because the diffusivity of product is much larger, however, P spreads noticeably by diffusion whereas the concentration profile of E·S is relatively sharp.

To compare the numerical calculations with the scaling predictions of the previous section, the numerically calculated concentrations of each species were integrated from $y = -w/2$

(15) Agah, A.; Aghajan, M.; Mashayekhi, F.; Amini, S.; Davis, R. W.; Plummer, J. D.; Ronaghi, M.; Griffin, P. B. *Nucleic Acids Res.* **2004**, *32*, e166.

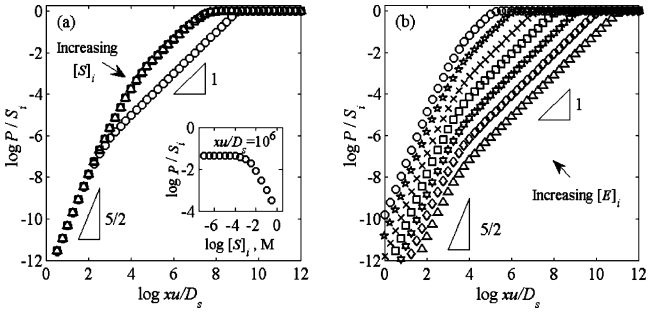

Figure 3. Numerical calculations of the integral product concentration (with units of moles, scaled on the initial moles of substrate concentration) as a function of downstream position in the channel. (a) Varied initial substrate concentration. Symbols: □, 10^{-7} M; △, 10^{-4} M; ○, 10^{-1} M. □ and △ are not differentiable at this scale. Inset: the integral production concentration at a fixed value of $xu/D_S = 10^6$ versus initial substrate concentration. (b) Varied initial enzyme concentration. Symbols in order from △ to ○ represent initial enzyme concentrations of 10^{-9}, 10^{-8}, 10^{-7} ... to 10^{-3} M, respectively.

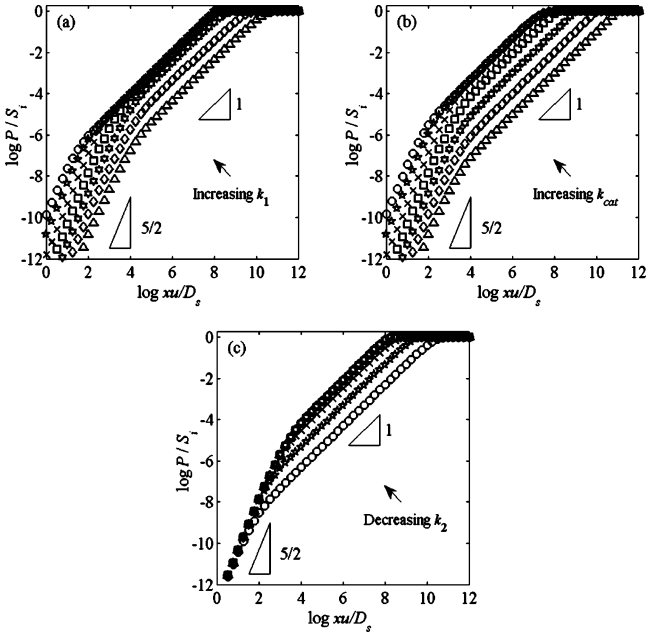

Figure 4. Numerical calculations of the integral product concentration (with units of moles, scaled on the initial moles of substrate concentration) as a function of downstream position in the channel. (a) Varied binding rate constant k_1. Symbols in order from △ to ○ represent, respectively, $k_1 = 10^1$, 10^2, ... to 10^7 M^{-1} s^{-1}. (b) Varied catalytic rate constant k_{cat}. Symbols in order from △ to ○ represent, respectively, $k_{cat} = 10^{-2}$, 10^{-1}, ... to 10^4 s^{-1}. (c) Varied reverse binding rate constant k_2. Symbols in order from △ to ○ represent, respectively, $k_2 = 10^{-3}$, 10^{-2}, ... to 10^3 s^{-1}.

to $y = +w/2$ using a standard quadrature routine. Here we focus on the product concentrations, since these are the most relevant experimentally. Figure 3a shows the influence of the initial substrate concentration (with all other parameters fixed) in logarithmic coordinates. For small values of x, the amount of product (scaled on the initial substrate concentration) is linear on a log−log plot with slope $^5/_2$, i.e., the product concentration increases as $x^{5/2}$ in accord with the theory introduced above. Note the scaled magnitude is invariant with initial substrate concentration at small x; although the total amount of product is increased for larger $[S]_i$, the relative proportion is unchanged.

The $x^{5/2}$ dependence of the product concentration persists for values of xu/D_S up to approximately 10^4, at which point the solution begins to bend over and the slope approaches 1, consistent with eq 14. For small values of $[S]_i$, the scaled downstream product concentration is similarly independent of $[S]_i$, as the curves collapse onto one another (Figure 3a). For a sufficiently high initial substrate concentration, however, the relative proportion of product begins to decrease. Physically, the relative decrease occurs because so much substrate is present that there is insufficient enzyme to yield an equivalent reaction rate. This behavior is captured in the inset of Figure 3a, which shows the scaled amount of product at a fixed value of x for different initial substrate concentrations. For small $[S]_i$, the scaled amount of product is invariant, but above a critical concentration the relative amount of product decreases. With regard to extracting the rate constant from the downstream product concentration, it is clear from Figure 3a that a high value of $[S]_i$ is preferable in terms of yielding a long linear regime.

The effect of initial enzyme concentration, with all other parameters fixed, is shown in Figure 3b. Not surprisingly, increases in enzyme concentration increase the amount of product formed at given values of x. Regardless of the enzyme concentration, however, the initial $x^{5/2}$ scaling is observed, which further corroborates the analytical results as described above. The downstream linear scaling is also observed, but in contrast to the effect of initial substrate concentration, the linear regime is most robust for very small values of $[E]_i$. Physically, if the initial enzyme concentration is high, a larger proportion of substrate is consumed near the entrance of the device before the species are well mixed. Thus, smaller enzyme concentrations are favorable for extracting kinetic parameters using the approach described here.

The influence of each kinetic rate constant is explored in Figure 4. The general trends of the initial $x^{5/2}$ scaling, followed by a transition to linear growth, are found in each case. For small x, increases in k_1 (Figure 4a) and k_{cat} (Figure 4b) both proportionally increase the amount of product at a given value of x, consistent with eq 12. At large x, however, increases in k_1 (or k_{cat}) eventually fail to raise the reaction rate, since the other reaction rate constant limits the overall rate of the reaction. In other words, the reaction rate saturates for sufficiently high values of either k_1 or k_{cat}. In contrast, the reverse binding constant k_2 has no effect on the initial rate of product formation at small x (Figure 4c). For sufficiently large values of k_2, the amount of product decreases, since the reverse reaction becomes favored.

EXPERIMENT

Methodology. The numerical calculations discussed above strongly corroborates the scaling analysis. To further test the predicted $x^{5/2}$ scaling, we performed a series of experiments in a Y-junction microfluidic channel using the bioluminescent reaction between adenosine triphosphate (ATP) and firefly luciferase/luciferin as a model system. Because of its high quantum yield and sensitivity to ATP, this reaction is widely used in biology to measure the concentration of ATP in solution.[16,17] The chemical

(16) Lundin, A.; Rickardsson, A.; Thore, A. *Anal. Biochem.* **1976**, *75*, 611.
(17) Lundin, A. Use of Firefly Luciferase in ATP-Related Assays of Biomass, Enzymes, and Metabolites. In *Bioluminescence and Chemiluminescence*, Part C; Academic Press Inc: San Diego, CA, 2000; Vol. 305, pp 346−370.

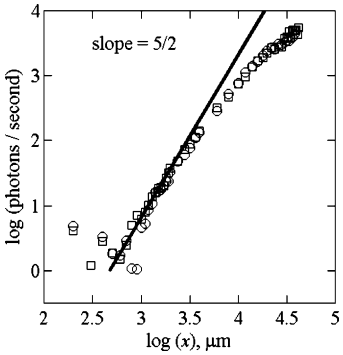

Figure 5. Experimental measurements of the light emitted by the reaction between luciferase and ATP as a function of position in the microchannel. A background signal of 8 photons/s was subtracted from the data. □ and ○ represent two different experiments under identical conditions. The solid line has a slope of $^5/_2$, in accord with the theory (cf. eq 12). Other experiments on other days also exhibited the slope of $^5/_2$.

reaction is described by

$$\mathrm{ATP} + \mathrm{LH_2} + \mathrm{E} \underset{k_2}{\overset{k_1}{\rightleftharpoons}} \mathrm{E{\cdot}LH_2{\cdot}ATP} \overset{k_{\mathrm{cat},2}}{\rightleftharpoons} \mathrm{E{\cdot}LH_2{\cdot}AMP} + \mathrm{PP_i}$$

$$\mathrm{E{\cdot}LH_2{\cdot}AMP} + \mathrm{O_2} \xrightarrow{k_{\mathrm{cat},2}} \mathrm{E{\cdot}L} + \mathrm{AMP} + \mathrm{CO_2} + h\nu \qquad (15)$$

where E represents luciferase, LH_2 is D-luciferin, L is dehydroluciferin, AMP is adenosine monophosphate, and PP_i represents inorganic pyrophosphates. Subsequent reactions after the light-emitting step ultimately release the enzyme. Clearly this reaction is more complicated than the standard Michaelis−Menten reaction; because the light-emitting species is depleted by subsequent reactions, a full comparison with the theoretical predictions for all x is precluded.

The reaction does have the feature, however, that an enzyme and substrate form an intermediate which subsequently gives off light. Moreover, by mixing luciferin and luciferase together prior to addition of ATP, the two effectively form a single enzymatic complex due to their high affinity for each other. In this situation, the reaction scheme (eq 15) can be simplified as

$$\mathrm{S} + \mathrm{E}^* \underset{k_2}{\overset{k_1}{\rightleftharpoons}} \mathrm{E}^*{\cdot}\mathrm{S} \xrightarrow{k_{\mathrm{cat},1}} \mathrm{P}^{(1)} \xrightarrow{k_{\mathrm{cat},2}} \mathrm{P}^{(2)} + h\nu \qquad (16)$$

where S is ATP, E* is the luciferin/luficerase complex, and $P^{(1)}$ and $P^{(2)}$ are the products described in eq 15. Thus, the rate of light production is given by

$$\frac{\mathrm{d}(h\nu)}{\mathrm{d}t} = k_{\mathrm{cat},2}[\mathrm{P}^{(1)}] \qquad (17)$$

In the context of the microfluidic approach, by the preceding analysis (cf. eq 12) we expect at small values of x that the concentration of $P^{(1)}$ will grow as

$$\mathrm{P}^{(1)} \propto k_1 k_{\mathrm{cat},1} x^{5/2} \qquad (18)$$

We therefore expect that the rate of photon emission $\mathrm{d}(h\nu)/\mathrm{d}t$ will initially increase as $x^{5/2}$, so counting photons versus position will serve as a test of the theory. Note, however, that the subsequent depletion of the product precludes comparison of the downstream data with eq 14. Therefore, the experiments we report here will serve simply to corroborate the predicted $x^{5/2}$ scaling result, rather than as a measurement of the rate constants themselves.

Firefly luciferase, ATP, and D-luciferin were purchased from Aldrich-Sigma. Physiological salt solution (PSS) was prepared as follows: 4.7 mM KCl, 2.0 mM $CaCl_2$, 1.2 mM $MgSO_4$, 140.5 mM NaCl, 21.0 mM tris(hydroxymethyl)aminomethane, and 11.1 mM dextrose with 5 mM bovine serum albumin. The pH was adjusted to 7.4. The luciferase/luciferin solution was prepared by adding 100 μL of 1 mg/mL luciferase and 2.5 mg of D-luciferin into 5 mL of PSS buffer. The ATP solution was prepared by adding 3 mg of ATP into 10 mL of deionized water and then diluted with PSS buffer to 420 μM. The luciferase/luciferin and ATP solution were always prepared on the day of use.

Microfluidic chips were fabricated in poly(dimethylsiloxane) (PDMS) using standard soft photolithography techniques. The system consisted of a Y-shaped microchannel, as depicted in Figure 1. The height and width of the main channel were 38 and 100 μm, respectively. The angle between the two arms of the chip was 90°. The ATP and preincubated luciferase/luciferin solution were injected at the same constant flow rate (3 μL/min) into the microdevice using a single syringe pump (Kd Scientific, KDS101). The flow rate in the main channel was thus 6 μL/min, corresponding to a mean velocity of 4 cm/s and a Reynolds number of approximately $\mathrm{Re} = uh/\nu \approx 2$ (where ν is the kinematic viscosity of the liquid), which indicates that the flow is laminar in this configuration.

The bioluminescent signal resulting from the luciferase reaction was measured in different downstream positions of the channel by translating a 100× objective (NA = 0.75) on a microscope (Leica DMIRB, Bannockburn, IL) along the length of the channel. The light signal was amplified by a photomultiplier tube (Hamamatsu, model R1527P, Japan) installed in a housing with a high-voltage power supply (Photon Technology International, model 814, Birmingham, NJ) and attached to the side of the microscope. The detected number of incident photons was recorded using a National Instruments data acquisition board and Labview software. Photons were counted for 30 s at each location and repeated five times before moving to the next detection area. Experiments were performed at room temperature (~25 °C) in a dark room; calibration trials in the absence of enzyme yielded a background intensity of 8 photons per second.

RESULTS

Representative results from two separate experiments conducted on the same day with the same batch of enzyme are presented in Figure 5. For the first 500 μm ($\log x < 2.7$), any signal resulting from the reaction is indistinguishable from the background intensity; the corrected photon intensity (i.e., signal minus background) fluctuates close to zero. Beginning around x = 500 μm, however, the amount of detected light increases. When

(18) Salmon, J. B.; Ajdari, A.; Tabeling, P.; Servant, L.; Talaga, D.; Joanicot, M. *Appl. Phys. Lett.* **2005**, *86*, 094106.

plotted logarithmically, the rate of photon emission clearly scales as $x^{5/2}$ for $x < 3000\ \mu$m (i.e., $\log x < 3.5$). Several other experiments yielded similar $x^{5/2}$ scaling, although the magnitude of the photon emission rate differed. These differences are presumably due to varying degrees of enzyme viability from one batch to another, as well as the lack of precise temperature control during the experiment.

The key point, however, is that the experimental results strongly corroborate the scaling predictions and the detailed numerical calculations. For even larger x, the rate begins to decrease and appears to approach a slope of 1, qualitatively in agreement with the behavior depicted in Figures 3 and 4. Not too much significance should be attached to this observation, however, since the true reaction (eq 15) involves subsequent reactions that deplete the amount of the light emitting species. Indeed, other experiments at even greater x showed that the rate of light emission decreased for sufficiently large x. This result is at odds with a pure Michaelis−Menten model but is consistent with the more complicated reaction scheme given in eq 15. For this reason, a quantitative extraction of the rate constants via the procedure outlined previously is not applicable. Nonetheless, the concentration of light-emitting species does scale as $x^{5/2}$ close to the entrance of the channel, in accord with the theory.

This agreement between theory and experiment might seem surprising, since the theory assumed uniform two-dimensional transport while the actual flow is three-dimensional. Indeed, previous work[12,13] on nonenzymatic reactions has indicated that the slower fluid velocity near the boundaries of the microchannel (i.e., $z = 0$, $z = h$) causes the transverse diffusive length scale to vary as $l_D \sim x^{1/3}$ rather than $x^{1/2}$ as observed in the bulk of the channel. One might expect the different power-law behavior near the boundaries to affect the spatial dependence of the product concentration, but the experimental results obtained here indicate that any such effect was negligible. According to Ismagilov et al., the relative proportion of fluid that obeys the $x^{1/3}$ scaling decreases as h decreases,[12] so presumably our experimental setup was thin enough that wall effects were diminished.

SUMMARY AND CONCLUSIONS

In summary, we established a simple method for interpreting experimental microfluidic data to determine rate constants for Michaelis−Menten reactions. Analytical, numerical, and experimental results all indicate that the concentration of product initially increases as $x^{5/2}$ along the length of the microchannel. This simple scaling provides a straightforward approach for extracting kinetic information from experimental data.

A key limitation of our experimental apparatus was its reliance on photon emission from a bioluminescent reaction. Few enzymatic reactions release light, so other methods of measuring concentration are desirable. For example, Salmon et al. incorporated Raman spectroscopy measurements into their microfluidic system.[18] Use of Raman spectroscopy, rather than photon counting, will greatly expand the number of reactions that may be analyzed using the approach advocated here.

We focused on enzymatic reactions that follow standard Michaelis−Menten kinetics to establish a limiting case for more complicated enzymatic reaction schemes, but we note that the methodology clearly applies to other systems with disparities in diffusivity. For example, reactions catalyzed by nanoparticles should behave similarly; a small reactant molecule introduced on one side of a Y-junction will diffuse rapidly toward the relatively slow nanoparticles introduced on the other side. Likewise, the theory can be extended to different geometries, such as junctions where three or more channels with different reactants converge. The effects of side reactions, reversibility, inhibitors, and other competing reactions remain to be considered. The results presented here serve as a framework to consider these complications.

ACKNOWLEDGMENT

We thank Harvard NSF-NSEC for support of this research.

Received for review December 3, 2007. Accepted January 20, 2008.

AC702469U